UDK 620.1:546.26:544.723.2:544.4:543.2
Original scientific article/Izvirni znanstveni članek

ISSN 1580-2949
MTAEC9, 55(3)449(2021)

PREPARATION AND CHARACTERIZATION OF ACTIVATED CARBON FROM OIL-PALM FIBER AND ITS EVALUATION FOR METHYLENE BLUE ADSORPTION

PRIPRAVA IN KARAKTERIZACIJA AKTIVIRANEGA OGLJIKA, IZDELANEGA IZ VLAKEN OLJNE PALME IN NJEGOVO OVREDNOTENJE S POMOČJO UPORABE POSTOPKA ADSORPCIJE METILENSKEGA MODRILA

Yuqi Wang[1], Jian Pan[3], Yanhui Li[1,2,*], Pengfei Zhang[1], Xiaoping Zhang[2], Meixiu Li[2], Heng Zheng[2], Yong Sun[1], Huimin Wang[1], Qiuju Du[2]

[1]College of Mechanical and Electrical Engineering, Qingdao University, Qingdao, China
[2]Laboratory of Fiber Materials and Modern Textile, Growing Base for State Key Laboratory, Qingdao University, Qingdao, China
[3]Xi'an Modern Control Technology Research Inevaluate it fortitute, Xi'an, China

Prejem rokopisa – received: 2020-04-23; sprejem za objavo – accepted for publication: 2021-03-19

doi:10.17222/mit.2020.068

A new type of activated carbon was produced from oil-palm fiber using steam activation. Scanning electron microscopy (SEM) was performed on the surface of oil-palm-fiber activated carbon (OPF-AC). The spectra of OPF-AC was investigated with Fourier-transform infrared (FTIR) spectroscopy. The effects of the temperature, adsorbent dose, adsorption time and pH on the adsorption properties of methylene blue on OPF-AC were discussed. The Langmuir adsorption model and Freundlich adsorption model were used to find the adsorption equilibrium isotherm. Adsorption kinetics were employed to explain the adsorption process and predict the adsorption efficiency. The Van't Hoff equation was used to assess the impact exerted by the adsorption temperature on the adsorbing process. According to the results, the data of the adsorption equilibrium of OPF-AC fit well the Langmuir adsorption model and the kinetics data can be gathered into a pseudo-second-order kinetic model. The adsorption behavior of methylene blue on OPF-AC was endothermic and spontaneous. The total pore volume and BET surface area of OPF-AC reached 0.7809 cm^3/g and 1018.84 m^2/g, respectively. The maximum adsorption capacity of OPF-AC was 862.07 mg/g at 323 K. Accordingly, the gratifying adsorption of OPF-AC endows it with a promising prospect in the application field of agricultural adsorbents.

Keywords: oil-palm-fiber activated carbon, steam activation, adsorption, methylene blue

Avtorji v pričujočem članku poročajo o novi vrsti z vodno paro aktiviranega ogljika, izdelanega iz vlaken oljne palme. Površino vlaken aktiviranega ogljika (OPF-AC) so okarakterizirali z vrstičnim elektronskim mikroskopom (SEM). Spekter OPF-AC so analizirali s Fourierjevo Transformacijsko Infrardečo (FTIR) spektroskopijo. Razpravljali so o vplivu temperature, doze adsorbenta, časa adsorpcije in kislosti (pH) na adsorpcijo metilenskega modrila na OPF-AC. S pomočjo Langmuirjevega in Freundlichovega modela adsorpcije so poizkušali najti ravnotežno izotermo adsorpcije. Kinetiko adsorpcije so uporabili za razlago adsorpcijskega procesa in njegove učinkovitosti. Van't Hoffovo enačbo so uporabili za oceno vpliva temperature na proces adsorpcije. V skladu z rezultati izvedenih analiz ugotavljajo, da se podatki za adsorpcijsko ravnotežje OPF-AC dobro ujemajo z Langmuirjevim adsorpcijskim modelom, podatki za kinetiko procesa pa se dobro ujemajo s pseudo kinetičnim modelom drugega reda. Adsorpcija metilenskega modrila na OPF-AC je bila spontana in endotermna. Izmerjeni celotni volumen por OPF-AC je bil 0,7809 cm^3/g, njihova površina preseka po BET je bila 1018,84 m^2/g. Maksimalna sposobnost za absorpcijo OPF-AC je bila pri 323 K enaka 862,07 mg/g. Rezultati raziskave kažejo, da se bodo lahko izdelani OPF-AC, zaradi dobrih adsorpcijskih lastnosti, uporabljali kot adsorbenti v kmetijstvu.

Ključne besede: aktivirano oglje, vlakna oljne palme, aktiviranje s paro, adsorpcija, metilensko modrilo

1 INTRODUCTION

As one of the main techniques for treating industrial wastewater to control environmental pollution, the activated carbon absorption method has several advantages, e.g., a low cost, simple operation, long service life and so on.[1] The choice of the natural precursor largely determines the adsorption capacity of activated-carbon products according to the available data (e.g., the size of particle, the size of pore and the area of surface). Activated carbons' natural precursors, which are cheap, local, effective and available, are being searched for continuously.

Using fully studied activation processes, activated carbons can be extracted from various precursors, e.g., natural materials, agricultural solid wastes, industrial solid waste and other miscellaneous adsorbents.[2] Agricultural and industrial wastes, used as activated-carbon precursor materials can be classified as low-cost and renewable materials. To obtain activated carbon, many types of agricultural/industrial solid wastes have been used to produce activated carbon with chemical activation, e.g., coconut shell,[3] peanut shell,[4] corn stover,[5] petroleum coke,[6] rattan sawdust,[7] jute fiber,[8] waste bio-

*Corresponding author's e-mail:
liyanhui537@163.com (Yanhui Li)

mass,[9] bituminous coal,[10] vetiver roots,[11] oil palm wood,[12] flamboyant pods,[13] dead leaves,[14] trichosanthes kirilowii maxim shell[15] and waste tea.[16] Though a literature survey on the adsorption of dye by biomass-activated carbon revealed a considerable number of relevant articles, the studies normally focus on the preparation of activated carbon through chemical activation.

As a common economic plant in south China, oil palm is widely distributed in Sichuan, Yunnan, Guizhou, Hunan and Hubei Province. Oil-palm fiber is an ideal activated-carbon precursor material due to its porous structure. As a wood fiber, oil-palm fiber has major research implications for environmental treatment. Thus, the innovation of this work is the pretreatment of oil-palm-fiber activated carbon (OPF-AC) with steam activation. Compared to the preparation with chemical activation, the OPF-AC prepared with steam activation exhibits many advantages, e.g., simple operation, cheap fabrication, low energy consumption and environmental friendliness.

Methylene blue (MB) is frequently used for producing printing inks and paints and dyeing leather, paper, silk and cotton. MB exhibits toxicity to the main microorganisms and cannot be easily removed from aqueous solutions. To assess the adsorption capacity of OPF-AC in removing hazardous materials from water, MB served as the adsorbate in our case. The adsorption behavior was systematically investigated in terms of the activation temperature, adsorption temperature, adsorbent dose, adsorption time and pH. The Freundlich adsorption model and Langmuir adsorption model aim to find the adsorption equilibrium isotherm. To explain the mechanism of the adsorption process and predict the adsorption efficiency, this study used the adsorption kinetics. The Van't Hoff equation was used to assess the impact exerted by the adsorption temperature on the adsorption process of OPF-AC.

2 EXPERIMENTAL PART

2.1 Chemicals and apparatus

MB was provided by Tianjin Guangcheng Chemical Reagent Co., Ltd., Tianjin, China. Oil-palm fiber was provided by Qingkang Co., Ltd., Pu'er, China. Other chemicals were obtained from Aladdin Industrial Co., Ltd., Shanghai, China. The reagents and solutions were prepared with distilled water. The absorbance of MB was tested with an ultraviolet–visible spectrophotometer. The maximum absorption wavelength of MB was 664 nm. The pore characteristics of OPF-AC were analyzed using nitrogen adsorption at 77 K (Micromeritics ASAP 2460). The surface feature of OPF-AC was analyzed with scanning electron microscopy (SEM, Helios Nanolab 600i, NEC Ltd., Japan). The functional groups of OPF-AC were tested with Fourier transform infrared (FTIR) spectroscopy (Nicolet iS50, Thermo Scientific, USA).

2.2 Preparation of OPF-AC

Oil-palm fiber was cut into 10–20 mm pieces and washed with distilled water. The treated oil-palm fiber was cured in an oven at 343 K for 24 h. The dried sample was carbonized in a tube furnace at 973 K under a purified nitrogen (99.995 %) flow. As the activation step, OPF-char was performed at different temperatures (973, 1023, 1073, 1123, 1173) K under purified nitrogen (99.995 %) and high-temperature steam flow. The N_2/H_2O ratio was 1:1. The activation time was set to 30 min. Next, OPF-AC materials were obtained and ground into powder.

2.3 Adsorption experiments

To produce a stock solution, 1000 mg of MB was dissolved in 1000 mL of deionized water. Then, different concentrations of the solution were diluted with the stock solution. The effect of the activation temperature (973, 1023, 1073, 1123, 1173) K of OPF-AC on the adsorption capacity was studied by adding 10 mg of OPF-AC into 20 mL of the MB solution at 308 K. The effect of the adsorbent dose (5, 10, 15, 20, 25, 30) mg on the adsorption capacity was tested by adding different doses of OPF-AC into the 20-mL MB solution at 308 K. The effect of the solution pH (3, 4, 5, 6, 7, 8, 9, 10) on the adsorption capacity was explored by adding 10 mg of OPF-AC into the 20-mL MB solution at 308 K. The impact exerted by the time of adsorbing the MB solution on the adsorption capacity was studied by adding 200 mg of OPF-AC into the 400-mL MB solution at 308 K. The MB concentration of the solution was 400 mg/L. The adsorption capacity was calculated as follows:

$$q_e = (c_0 - c_e) \times V/W \quad (1)$$

$$q_t = (c_0 - c_t) \times V/W \quad (2)$$

where q_e is the adsorption capacity (mg/g), q_t is the adsorption capacity at time t (mg/g), c_t is the MB concentration at time t (mg/L), c_0 is the initial MB concentration (mg/L), c_e is the equilibrium MB concentration (mg/L), V is the MB solution volume and W is the mass of OPF-AC.

The Langmuir model (Equations (3) and (4)) and Freundlich model (Equation (5)) are employed for exploring the adsorption equilibrium isotherm. In the Langmuir model, the adsorption process is assumed to occur on a uniform surface.[17] The plot of c_e/q_e vs c_e yields a linear graph with slope $1/q_{max}$. The Langmuir constant, k_L, can be calculated from the intercept on the y-axis. In the Freundlich model, the adsorption is assumed to occur on a heterogeneous surface.[18,19] The plot of $\ln q_e$ vs $\ln c_e$ generates a linear graph with the $1/n$ slope. $\ln k_F$ can be calculated from the intercept on the y-axis.

$$c_e/q_e = c_e/q_{max} + 1/q_{max}k_L \quad (3)$$

$$R_L = 1/(1 + c_0 k_L) \quad (4)$$

$$\text{Ln } q_e = \ln k_F + \ln c_e/n \quad (5)$$

Here, k_F is the Langmuir constant, c_e is the equilibrium concentration, q_e is the amount adsorbed at equilibrium, q_{max} is the maximum adsorption capacity of the complete monolayer coverage and R_L is the dimensionless equilibrium parameter. If the R_L value is $0 < R_L < 1$, the Langmuir isotherm is favorable. k_F is the Freundlich constant correlated with the adsorption capacity and n is the Freundlich constant correlated with the adsorption intensity.

2.4 Adsorption-kinetic models

To predict the adsorption efficiency and explain the mechanism of the adsorption process, the adsorption kinetics is used. There are three continuous mass-transport steps in the kinetic mechanism of adsorption, which can be tested with three kinetic models (intra-particle diffusion equation, pseudo-second-order equation and pseudo-first-order equation).

The following Equation (6) is pseudo-first-order equation.[20] The plot of $\log(q_e - q_t)$ vs t generates a linear graph with the $k_1/2.303$ slope. q_e can be calculated from the intercept on the y-axis.

$$\log(q_e - q_t) = \log q_e - t \times k_1/2.303 \quad (6)$$

Here, k_1 is the rate constant of the pseudo-first-order, q_t is the adsorption capacity at time t, q_e is the adsorption capacity at equilibrium.

Equation (7) is a pseudo-second-order equation.[21] The plot of $1/q_t$ vs t generates a linear graph with the $1/q_e$ slope. k_2 can be calculated from the intercept on the y-axis.

$$t/q_t = t/q_e + 1/(k_2 q_e^2) \quad (7)$$

Here, k_2 is the rate constant of the pseudo second order.

Equation (8) is an intra-particle diffusion equation. The plot of q_t vs $t^{1/2}$ generates a linear graph with the k_{id} slope. c_i is calculated from the intercept on the y-axis.

$$q_t = k_{id} t^{1/2} + c_i \quad (8)$$

Here, $t^{1/2}$ is the square root of the time, k_{id} is the rate constant of the intra-particle diffusion and c_i is the larger effect of the boundary layer upon molecular diffusion.

2.5 Thermodynamic study

The Van't Hoff equation aims at the investigation of the impact exerted by the temperature of the MB adsorbing process onto OPF-AC.[22–24] The plot of $\ln(q_e/c_e)$ vs $1/T$ generates a linear graph with the $\Delta H/R$ slope. $\Delta S/R$ is calculated from the intercept on the y-axis.

$$\ln(q_e/c_e) = -\Delta H/(RT) + \Delta S/R \quad (9)$$

$$\Delta G = \Delta H - T\Delta S \quad (10)$$

Here, q_e is the adsorption capacity at equilibrium, c_e is the MB concentration at equilibrium, ΔG is the variation of Gibbs free energy, ΔS is the variation of entropy, ΔH is the variation of enthalpy, T is the temperature in Kelvin and R is the ideal gas constant (8.314 J/mol K).

3 RESULTS AND DISCUSSION

3.1 Selection of the activation temperature

Figures 1a and **1b** show the effect of the activation temperature on the transformation rate and adsorbing ability of OPF-AC. Obviously, as the temperature for activation rises, the transformation rate of OPF-AC is down-regulated. The maximum transformation rate of OPF-AC is 39.74 % at 973 K. The minimum transformation rate of OPF-AC is 2.62 % at 1173 K. The OPF-AC adsorption capacity increases as the activation temperature rises. The maximum adsorption capacity of OPF-AC is 599.696 mg/g at 1173 K. The minimum adsorption capacity of OPF-AC is 124.98 mg/g at 973 K. However, the transformation rate of OPF-AC is 16.24 %, and the adsorption capacity of OPF-AC reaches 598.766 mg/g (the standard deviation = 24.378) at an activation temperature of 1123 K. The OPF-AC produced at 1123 K not only exhibits high absorption ability but also a high production. Thus, the OPF-AC produced at 1123 K was

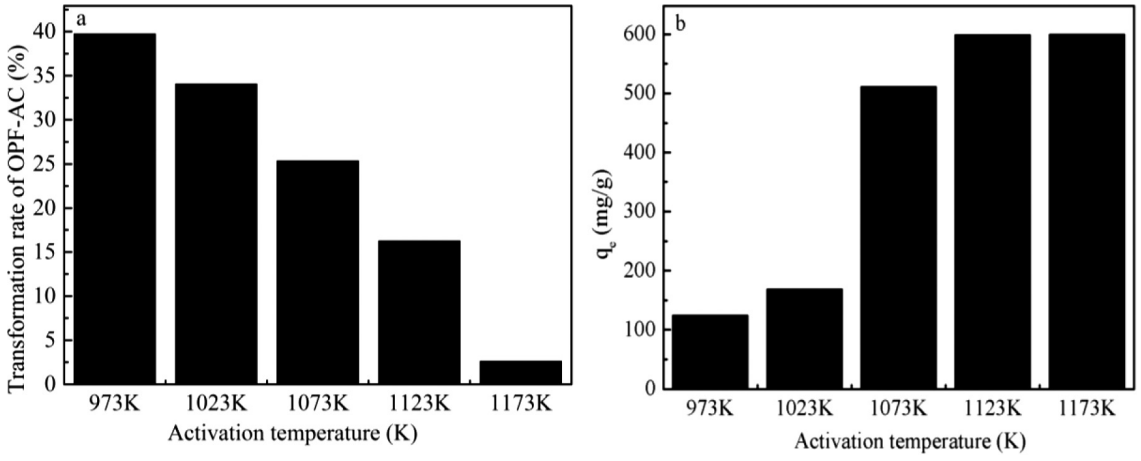

Figure 1: Effect of the activation temperature on the transformation rate and adsorption capacity of OPF-AC: a) transformation rate of OPF-AC, b) adsorption capacity

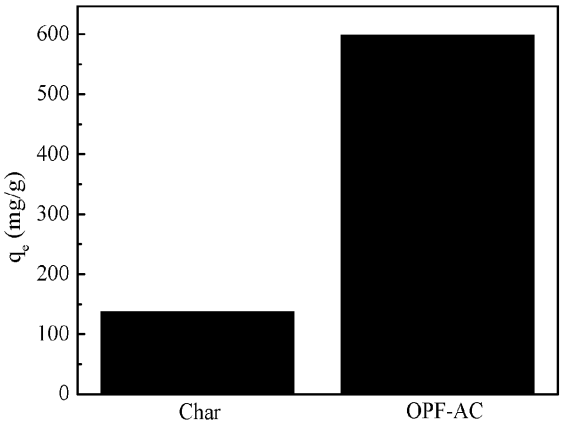

Figure 2: Comparison of the adsorption capacity of OPF-char and OPF-AC

used for the adsorption experiment here. **Figure 2** shows that the adsorption ability of OPF-AC is greater than the adsorption capacity of OPF-char. In the adsorption tests, the OPF-AC used is 10 mg in weight. For the concentration solution, the concentration reaches 300 mg/L.

3.2 Characterizations of OPF-AC

SEM images of the surface features of OPF-char and OPF-AC were taken. **Figures 3a** and **3b** show the surface morphologies of OPF-char at 973 K. **Figures 3c** and **3d** show the surface morphologies of OPF-AC at 1123 K. The surface of OPF-AC is markedly porous, with all sorts of irregular cavities.

Figure 4 shows the nitrogen adsorption/desorption isotherms of OPF-char and OPF-AC. Porous characteristic parameters, including the BET surface area, total pore volume determined at relative pressure $p/p_o = 0.99$, t-Plot micropore volume, mesopore volume and Barrett-Joyner-Halenda (BJH) desorption average pore size are listed in **Table 1**. The BET surface area of OPF-AC was 1018.84 m^2/g. The total pore volume of OPF-AC was 0.7809 cm^3/g. The micropore volume of OPF-AC was 0.2393 cm^3/g. The mesopore volume reached 0.5416 cm^3/g. Compared to the porous characteristic parameters of OPF-char, the mesopore volume, micropore volume, total pore volume and BET surface area increased to 555.75 m^2/g, 0.5348 cm^3/g, 0.0457 cm^3/g, and 0.4891 cm^3/g, respectively.

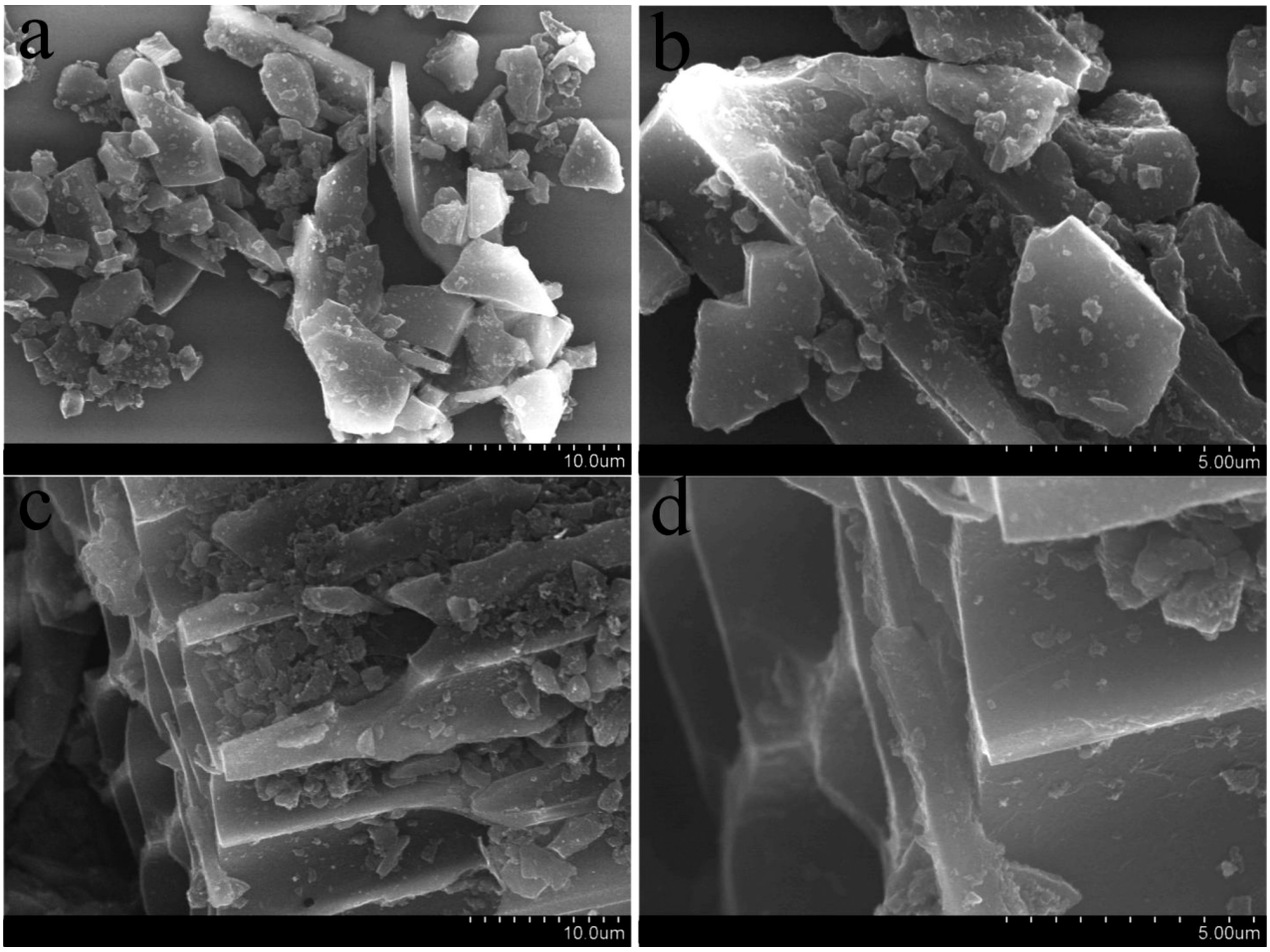

Figure 3: SEM images of OPF-char and OPF-AC: a) and b) SEM images of OPF-char, c) and d) SEM images of OPF-AC

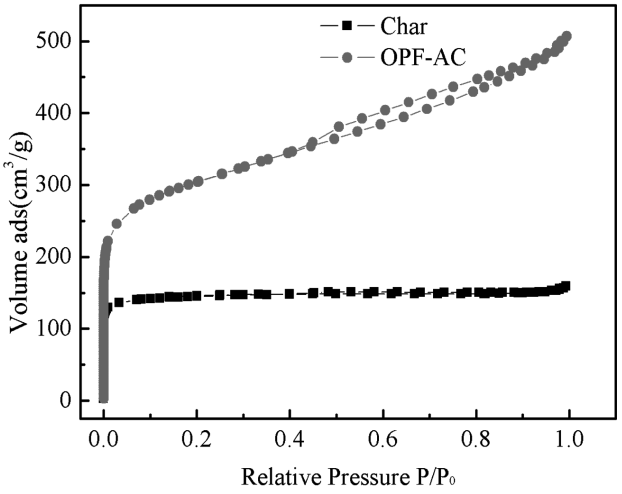

Figure 4: Nitrogen adsorption/desorption isotherms of OPF-char and OPF-AC

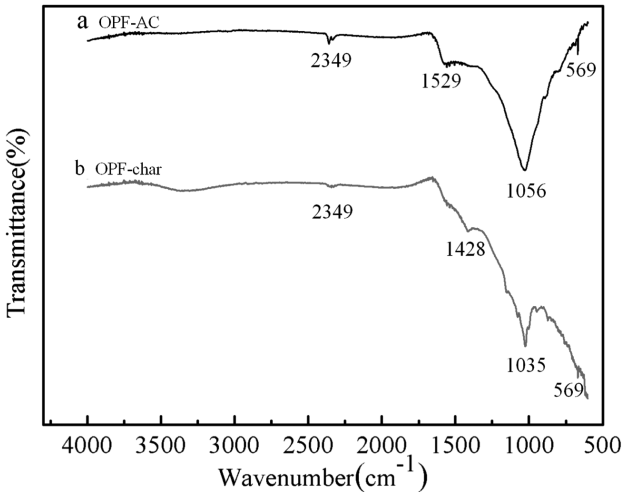

Figure 5: FTIR spectrum of OPF-char and OPF-AC

Table 1: Porous characteristic parameters of OPF-AC and OPF-char

Sample	BET surface area (m^2/g)	Total pore volume (cm^3/g)	Micropore volume (cm^3/g)	Mesopore volume (cm^3/g)	Average pore size (nm)
OPF-char	463.09	0.2461	0.1936	0.0525	5.2
OPF-AC	1018.84	0.7809	0.2393	0.5416	4.7

To explore the functional groups of OPF-char and OPF-AC, OPF-char and OPF-AC were tested with Fourier transform infrared (FTIR) spectroscopy as shown in **Figure 5**. The FTIR spectrum of OPF-char shows peaks at (2349, 1428, 1035 and 569) cm^{-1}, following the presence of C=C (alkyne), C-O-C (ester, ether and phenol), -CN_2 (alkyl) as well as C-H.[25] The FTIR spectrum of OPF-AC shows peaks at (2349, 1529, 1056, 569) cm^{-1}, corresponding to the existence of C=C (alkyne), C-O-C (ester, ether and phenol), -NO_2 (alkyl) as well as C-H.[25]

3.3 Impact of different experimental parameters on the MB adsorption

The temperature not only affects the physicochemical properties of the adsorbent, but also affects its diffusing rate. Accordingly, exploring the effect of temperature upon the adsorption process of OPF-AC is necessary. The adsorption temperatures were defined at (293, 308, 323) K. Through three parallel experiments, analyzing the experiment data and phenomena, the adsorption curves were obtained. **Figure 6a** shows that the adsorption capacity of OPF-AC reaches 799.728 mg/g at 293 K while pH = 6. The OPF-AC adsorption capacity reaches 829.444 mg/g at 308 K. The OPF-AC adsorption capacity reaches 859.424 mg/g at 323 K. Increasing adsorption temperature increased the OPF-AC adsorption capacity. In the adsorption tests, the OPF-AC weight used was 10 mg. For the MB concentration solution, the concentration rose from 300 mg/L to 450 mg/L.

With the increase in the adsorbent dose, the effects of the adsorbent dose upon the OPF-AC removal percentage and adsorption capacity are explored, as shown in **Figure 6b,** with pH = 6. Increasing the adsorbent dose reduced the adsorption capacity. Since the amount of dye adsorbed per unit weight of adsorbent was reduced, the utilization ratio of active sites decreased. Increasing the adsorbent dose up-regulated the removal percentage at the initial phases due to numerous active adsorption sites.[26] Besides, the adsorbent dose up-regulated furtherly, whereas the removal percentage was found to increase only slightly, as the adsorption sites could not be available due to the saturation.[27] In the adsorption tests, the MB concentration of the solution was 400 mg/L. For the adsorbent dose, the weight increased from 5 mg to 30 mg.

Figure 6c shows that because of the available adsorbent surface area and many vacant adsorption sites, the MB adsorption rate increased fast in the initial phases, with pH = 6. Over time, the adsorption rate of MB slowed down sharply and then became constant. When this constant rate was exceeded, no more MB could be removed from the solution in nearly 370 min. In the meantime, the amount of the dye desorbed from the activated carbon reached dynamic equilibrium with the amount of the dye adsorbed onto the activated carbon.[28] In the adsorption tests, the effect of the adsorption time of MB solutions on the adsorption capacity was studied by adding 200 mg of OPF-AC into the 400-mL MB solution. The MB concentration of the solution reached 400 mg/L.

Figure 6d shows the effect of the solution pH (a pH range from 3–10) upon the MB removal by OPF-AC. The OPF-AC weight used was 10 mg. The maximum MB removal percentage was 99.95 % at pH = 10. The minimum MB removal percentage was 92.12 % at pH = 2. When the solution pH rose from 3 to 7, the MB removal percentage was up-regulated dramatically. When the solution pH rose from 7 to 10, the MB removal percentage was up-regulated slightly. **Figures 7a** to **7c** show the possible mechanism of the interaction of OPF-AC with

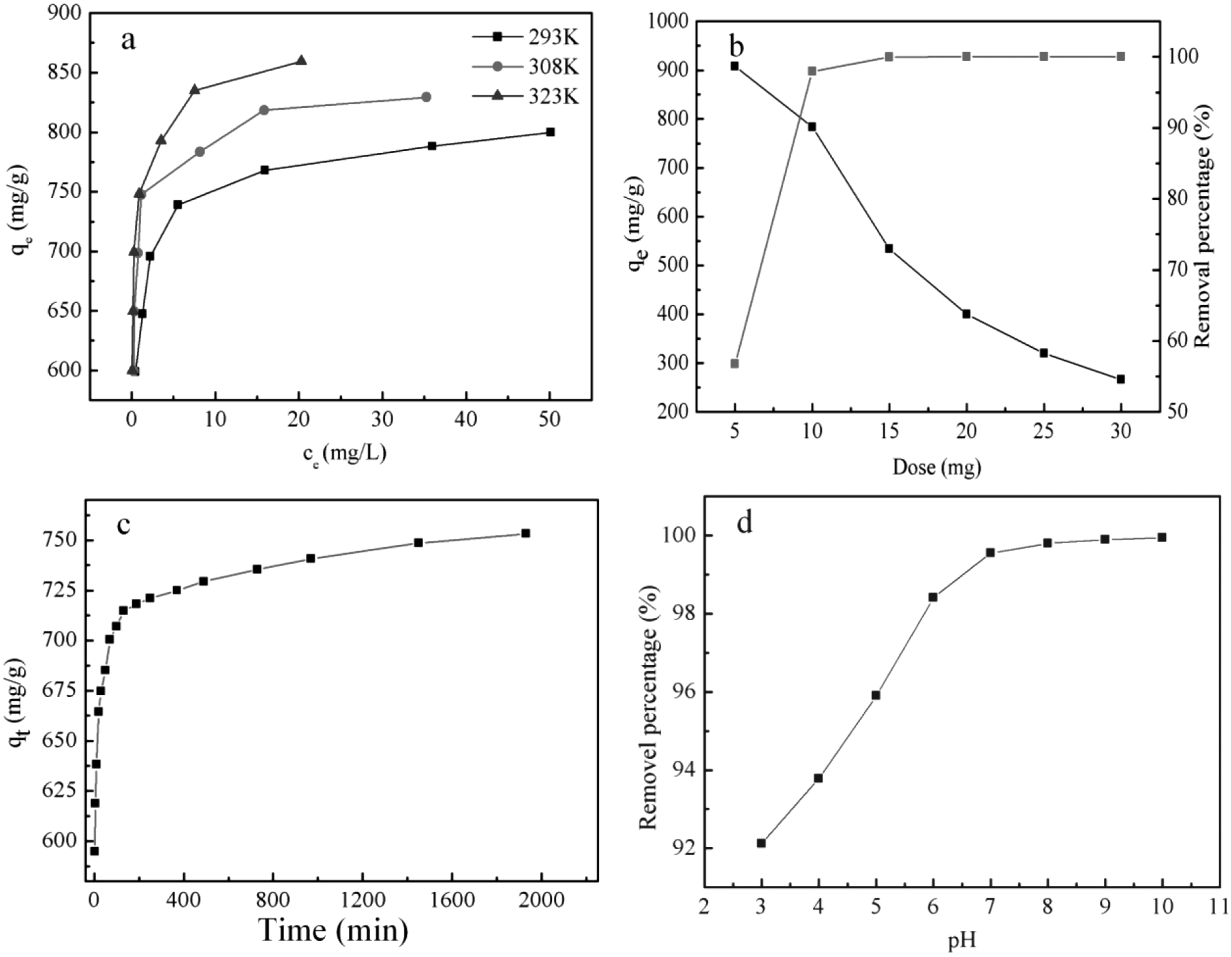

Figure 6: Adsorption affected by different factors: a) temperature, b) dose, c) adsorption time, d) pH

MB dye molecules under different pH conditions.[29] At lower pH values, hydroxyl and carboxyl functional groups on the surface of OPF-AC were protonated and became more positively charged. The adsorption efficiency was thus reduced owing to the significant electrostatic repulsion between the MB molecules and OPF-AC, both of which were charged positively. In the case of higher pH values, because of the increased number of negatively charged groups, the carboxyl and hydroxyl groups of OPF-AC were deprotonated, tending to be incorporated into the MB molecules. Accordingly, increasing the solution pH up-regulated the MB-removal percentage because of the competitive adsorption between hydrogen ions and MB molecules upon available binding sites. In the meantime, deprotonation of OPF-AC could interact with MB and improve the adsorption capacity of MB. In the adsorption tests, 10 mg of OPF-AC was used. For the MB concentration solution, the concentration was 400 mg/L.

3.4 Adsorption isotherms

Describing adsorption mechanism between MB and OPF-AC is necessary. **Figures 8a** and **8b** show that to analyze the experimental data, the Langmuir and Freundlich isotherm models were used and plotted at (293, 308, 323) K, respectively. The parameters are

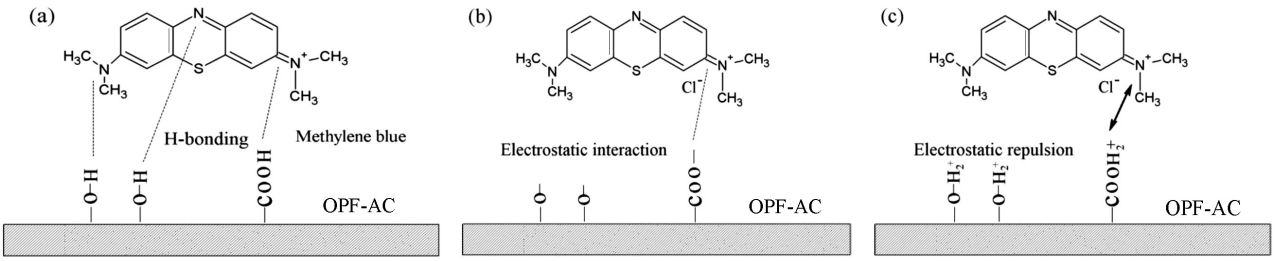

Figure 7: OPF-AC and MB interaction under different pH conditions: a) neutral; b) alkaline; and c) acidic

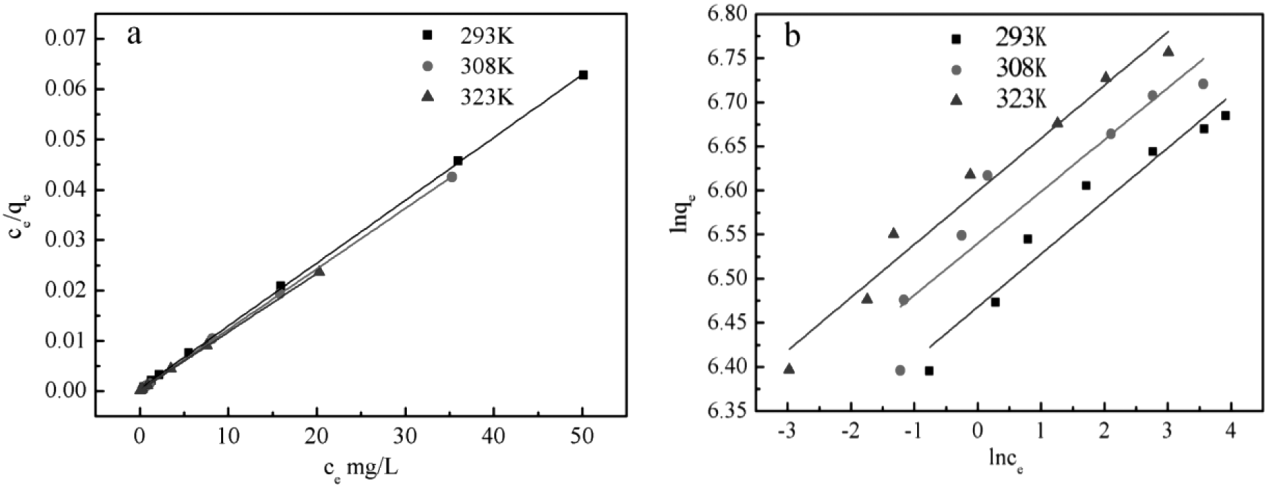

Figure 8: Adsorption equilibrium isotherm models: a) Langmuir model, b) Freundlich model

shown in **Table 2**. The maximum adsorption capacity of OPF-AC was 862.07 mg/g at 323K. R^2 is the correlation coefficient, indicating whether the Freundlich model and Langmuir model are appropriate to describe the MB adsorption equilibrium with OPF-AC. The results reveal that the Langmuir model is suitable for describing the MB adsorption equilibrium. Accordingly, it is concluded that the surface is homogenous, and the dye molecules adsorbed showed a monolayer on the OPF-AC surface. The maximum adsorption capacity of OPF-AC was compared to those of the other activated carbons, listed in **Table 3**. The maximum adsorption capacity of OPF-AC is lower than that of flamboyant-pod activated carbon. However, it is higher than those of the other activated carbons. Though OPF-AC has lower maximum adsorption capacity than flamboyant-pod activated carbon, the method for preparing OPF-AC is simple and environment-friendly, having a short reaction and mild reaction temperature without the need to use a chemical reagent during the activation.

3.5 Kinetic studies

To understand the adsorption dynamics according to the adsorbate's mass transfer and contact time, it is necessary to determine the adsorption kinetics.[30,31] To predict the adsorption efficiency and explain the mechanism of the adsorption process, as shown in **Figures 9a** to **9c**, the adsorption kinetics was used. The values yielded with Equations (6), (7) and (8) during the study of the adsorption mechanism with kinetic models (pseudo-first-order, pseudo-second-order and intra-particle diffusion) are listed in **Table 4**. The correlation coefficient in Equation (6) is 0.6717, suggesting that the MB adsorp-

Table 2: Calculation parameters of adsorption equilibrium isotherm models

T/K	Langmuir				Freundlich		
	q_{max} (mg/g)	k_L (L/mg)	R^2	R_L	k_F (L/mg)	1/n	R^2
293	800	0.389	0.99985	0.0084	644.1618	0.06013	0.94049
308	833.33	0.191	0.99984	0.0171	692.3350	0.05873	0.84878
323	862.07	0.125	0.99974	0.0260	734.3531	0.06013	0.96487

Table 3: MB adsorption capacity of various activated carbons

Dyes	Adsorbent	Experimental conditions				
		Dose (g/L)	pH	*T* (K)	Concn (mg/L)	q_{max} (mg/g)
MB	OPF-AC	0.5	6	323	300–450	862.07
MB	Rattan-sawdust activated carbon[7]	1	N/A	303	100–500	294.12
MB	Jute-fiber carbon[8]	1.5	4	301	50–500	225.64
MB	Waste-biomass activated carbon[9]	2	6	298	0–250	16.43
MB	Steam-activated bituminous coal[10]	1	7	293	100–800	588
MB	Vetiver-root activated carbon[11]	0.1	N/A	298	50–300	526
MB	Oil-palm-wood activated carbon[12]	1	N/A	303	10–250	90.9
MB	Flamboyant-pod activated carbon[13]	1	6.5	298	800–1000	895
MB	Dead-leaf activated carbon[14]	5	6.5	318	250–750	285
MB	Optimized waste-tea activated carbon[16]	1	2	323	50–350	554.3

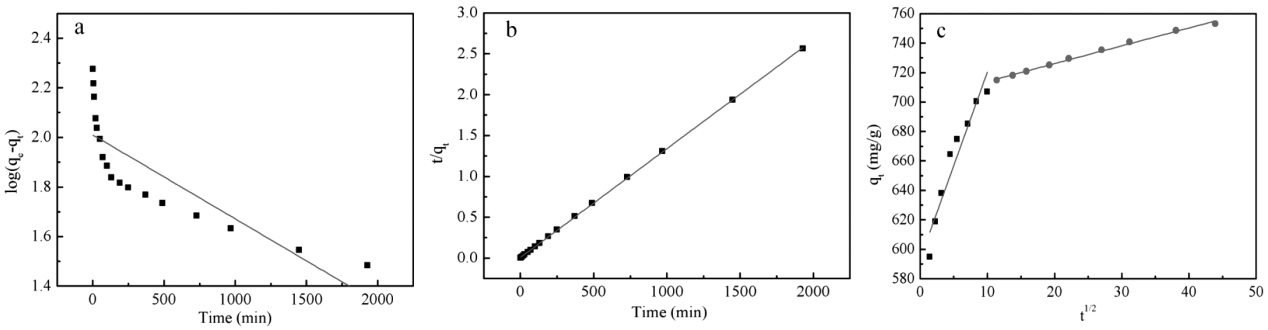

Figure 9: Adsorption kinetics models: a) pseudo-first-order, b) pseudo-second-order, c) intraparticle diffusion

tion to OPF-AC is not in conformity with the pseudo-first-order kinetic model. The correlation coefficient in Equation (7) is 0.9999. The adsorption capacity is calculated as 751.88 mg/g. Experimentally, the adsorption capacity is 783.61 mg/g. Thus, the MB adsorption to OPF-AC conforms to the pseudo-second-order kinetic model. The correlation coefficient of Equation (8) is lower than that of Equation (7). The above information suggests that the adsorption of MB onto OPF-AC is a complicated process, and intraparticle diffusion is not the mere rate-controlling step.

Table 4: Calculation parameters of the adsorption-kinetic models

Kinetic model	Parameters	Values
Pseudo-first-order	k_1 (min^{-1})	0.78×10^{-3}
	q_e (mg/g)	102.25
	R^2	0.6717
Pseudo-second-order	k_2	0.21×10^{-3}
	q_e	751.88
	R^2	0.9999
Intraparticle diffusion model	k_{id1}	1.2081
	c_1	701.91
	R_1^2	0.9941
	k_{id2}	12.6576
	c_2	593.67
	R_2^2	0.9132

3.6 Thermodynamic studies

The Van't Hoff equation was used to investigate the effect of temperature upon the MB adsorption onto OPF-AC.[22] The correlation coefficient is 0.9833.

Table 5: Parameter values for the Van't Hoff equation

T/K	ΔG	ΔH	ΔS
293K	–10.12	0.001699	0.03454
308K	–10.64		
323K	–11.15		

Table 5 shows the parameter values of the Van't Hoff equation. The value of ΔG is negative (–10.12, –10.64, –11.15), suggesting that MB adsorption onto OPF-AC is spontaneous and feasible. The value of ΔH *i*s positive (0.001699), revealing that the MB adsorption onto OPF-AC is an endothermic processes. The value of ΔS is positive (0.03454), confirming the improvement in the adsorption at the solid-solute interface.

4 CONCLUSIONS

In this study, the authors produced a novel activated carbon using oil-palm fiber and steam activation. Compared to the preparation with chemical activation, the OPF-AC prepared with steam activation exhibits many advantages, e.g., simple operation, cheap fabrication, low energy consumption and environmental friendliness. Compared to the other biological activated carbons, OPF-AC has a better adsorption capacity. A SEM analysis reveals that the surface of OPF-AC was markedly porous and widely covered with all sorts of irregular cavities. Subsequently, the effects of different experimental parameters (adsorption time, pH, adsorbent dose and temperature) upon the MB adsorption onto OPF-AC were studied. The MB adsorption onto OPF-AC follows the pseudo-second-order kinetic model. The Langmuir model is suitable for describing the adsorption equilibrium. The total pore volume and BET surface area of OPF-AC were 0.7809 cm^3/g and 1018.84 m^2/g, respectively. The maximum adsorption capacity of OPF-AC was 862.07 mg/g at 323 K. The Van't Hoff equation was used to assess the effect of temperature upon the MB adsorption onto OPF-AC, suggesting that the MB adsorption onto OPF-AC is endothermic and spontaneous.

Acknowledgments

This study was supported by the National Natural Science Foundation of China (No.51672140), Taishan Scholar Program of Shandong Province (No.201511029), Science and Technology Support Plan for Youth Innovation of Colleges in Shandong Province (DC2000000891) and Natural Science Foundation of Shandong Province (ZR2020QE016).

5 REFERENCES

[1] J. Labanda, J. Sabaté, J. Llorens, Modeling of the dynamic adsorption of an anionic dye through ion-exchange membrane adsorber, J. Membr. Sci., 340 (**2009**), 234–240, doi:10.1016/j.memsci.2009.05.036

[2] S. J. Allen, L. Whitten, G. Mckay, The production and characterisation of activated carbons: a review, Asia-Pac. J. Chem. Eng., 6 (**2010**) 5, 231–261, doi:10.1002/apj.5500060501

[3] A. M. Aljeboree, A. N. Alshirifi, A. F. Alkaim, Kinetics and equilibrium study for the adsorption of textile dyes on coconut shell activated carbon, Arabian J. Chem., 10 (**2017**), 3381–3393, doi:10.1016/j.arabjc.2014.01.020

[4] Z. A. Al-Othman, R. Ali, M. Naushad, Hexavalent chromium removal from aqueous medium by activated carbon prepared from peanut shell: adsorption kinetics, equilibrium and thermodynamic studies, Chem. Eng. J., 184 (**2012**), 238–247, doi:10.1016/j.cej.2012.01.048

[5] F. Shen, Y. Wang, L. Li, K. Zhang, R. L. Smith, X. Qi, Porous carbonaceous materials from hydrothermal carbonization and KOH activation of corn stover for highly efficient CO_2 capture, Chem. Eng. Commun., 205 (**2018**) 4, 423–431, doi:10.1080/00986445.2017.1367671

[6] X. Yuan, S. W. Choi, E. Jang, K. B. Lee, Chemically activated microporous carbons derived from petroleum coke: Performance evaluation for CF_4 adsorption, Chem. Eng. J., 336 (**2018**), 297–305, doi:10.1016/j.cej.2017.11.168

[7] B. H. Hameed, A. L. Ahmad, K. N. A. Latiff, Adsorption of basic dye (methylene blue) onto activated carbon prepared from rattan sawdust, Dyes Pigm., 75 (**2007**) 1, 143–149, doi:10.1016/j.dyepig.2006.05.039

[8] S. Senthilkumaar, P. R. Varadarajan, K. Porkodi, C. V. Subbhuraam, Adsorption of methylene blue onto jute fiber carbon: kinetics and equilibrium studies, J. Colloid Interface Sci., 284 (**2005**) 1, 78–82, doi:10.1016/j.jcis.2004.09.027

[9] S. Karagöz, T. Tay, S. Ucar, M. Erdem, Activated carbons from waste biomass by sulfuric acid activation and their use on methylene blue adsorption, Bioresour. Technol., 99 (**2008**) 14, 6214–6222, doi:10.1016/j.biortech.2007.12.019

[10] E. N. E. Qada, S. J. Allen, G. M. Walker, Adsorption of Methylene Blue onto activated carbon produced from steam activated bituminous coal: A study of equilibrium adsorption isotherm, Chem. Eng. J., 124 (**2006**) 1, 103–110, doi:10.1016/j.cej.2006.08.015

[11] S. Altenor, B. Carene, E. Emmanuel, J. Lambert, J. J. Ehrhardt, S. Gaspard, Adsorption studies of methylene blue and phenol onto vetiver roots activated carbon prepared by chemical activation, J. Hazard. Mater., 165 (**2009**) 1, 1029–1039, doi:10.1016/j.jhazmat.2008.10.133

[12] A. L. Ahmada, M. M. Loha, J. A. Azizb, Preparation and characterization of activated carbon from oil palm wood and its evaluation on Methylene blue adsorption, Dyes Pigm., 75 (**2007**) 2, 263–272, doi:10.1016/j.dyepig.2006.05.034

[13] A. M. M. Vargas, A. L. Cazetta, M. H. Kunita, T. L. Silva, V. C. Almeida, Adsorption of methylene blue on activated carbon produced from flamboyant pods (Delonix regia): study of adsorption isotherms and kinetic models, Chem. Eng. J., 168 (**2011**) 2, 722–730, doi:10.1016/j.cej.2011.01.067

[14] M. U. Dural, L. Cavas, S. K. Papageorgiou, F. K. Katsaros, Methylene blue adsorption on activated carbon prepared from Posidonia oceanica (L.) dead leaves: kinetics and equilibrium studies, Chem. Eng. J., 168 (**2011**) 1, 77-85, doi:10.1016/j.cej.2010.12.038

[15] Y. Wang, Y. Li, H. Zheng, Equilibrium, kinetic and thermodynamic studies on methylene blue adsorption by Trichosanthes kirilowii Maxim shell activated carbon, Pol. J. Chem. Technol., 21 (**2019**) 4, 89–97, doi:10.2478/pjct-2019-0044

[16] M. Auta, B. H. Hameed, Optimized waste tea activated carbon for adsorption of Methylene Blue and Acid Blue 29 dyes using response surface methodology, Chem. Eng. J., 175 (**2011**) 8, 233–243, doi:10.1016/j.cej.2011.09.100

[17] L. Li, L. Fan, M. Sun, H. Qiu, X. Li, H. Duan, C. Luo, Adsorbent for chromium removal based on graphene oxide functionalized with magnetic cyclodextrin-chitosan, Int. J. Biol. Macromol., 58 (**2013**) 7, 169–175, doi:10.1016/j.colsurfb.2013.01.074

[18] V. K. Gupta, D. Pathania, S. Sharma, S. Agarwal, P. Singh, Remediation of noxious chromium (VI) utilizing acrylic acid grafted lignocellulosic adsorbent, J. Mol. Liq., 177 (**2013**) 1, 343–352, doi:10.1016/j.molliq.2012.10.017

[19] Y. Wang, Y. Li, H. Li, H. Zheng, Q. Du, Equilibrium, kinetic and thermodynamic studies on methylene blue adsorption by konjac glucomannan/activated carbon aerogel, J. Polym. Environ., 27 (**2019**), 1342–1351, doi:10.1007/s10924-019-01420-3

[20] M. Doğan, M. Alkan, Ö. Demirbaş, Y. Özdemir, C. Özmetin, Adsorption kinetics of maxilon blue GRL onto sepiolite from aqueous solutions, Chem. Eng. J., 124 (**2006**) 1, 89–101, doi:10.1016/j.cej.2006.08.016

[21] Y. S. Ho, C. C. Chiang, Sorption studies of acid dye by mixed sorbents, Adsorption – journal of the International Adsorption Society, 7 (**2001**) 2, 139–147, doi:10.1023/A:1011652224816

[22] P. K. Neghlani, M. Rafizadeh, F. A. Taromi, Preparation of aminated-polyacrylonitrile nanofiber membranes for the adsorption of metal ions: comparison with microfibers, J. Hazard. Mater., 186 (**2011**) 1, 182–189, doi:10.1016/j.jhazmat.2010.10.121

[23] Y. Wang, Y. Li, X. Zhang, H. Zheng, Removal of methylene blue from water by copper alginate/activated carbon aerogel: equilibrium, kinetic, and thermodynamic studies, J. Polym. Environ., 28 (**2019**) 1, 200–210, doi:10.1007/s10924-019-01577-x

[24] M. K. Purkait, A. Maiti, S. Dasgupta, S. De, Removal of congo red using activated carbon and its regeneration, J. Hazard. Mater., 145 (**2007**) 1, 287–295, doi:10.1016/j.jhazmat.2006.11.021

[25] Rahmi, Lelifajri, Julinawati, Shabrina, Preparation of chitosan composite film reinforced with cellulose isolated from oil palm empty fruit bunch and application in cadmium ions removal from aqueous solutions, Carbohydr. Polym., 170 (**2017**), 226–233, doi:10.1016/j.carbpol.2017.04.084

[26] N. Song, X. L. Wu, S. Zhong, H. Lin, J. R. Chen, Biocompatible G-Fe_3O_4/CA nanocomposites for the removal of methylene blue, J. Mol. Liq., 212 (**2015**), 63–69, doi:10.1016/j.molliq.2015.08059

[27] V. K. Gupta, R. Jain, M. N. Siddiqui, T. A. Saleh, S. Agarwal, S. Malati, D. Pathak, Equilibrium and thermodynamic studies on the adsorption of the dye rhodamine-B onto mustard cake and activated carbon, J. Chem. Eng. Data, 55 (**2010**) 11, 5225–5229, doi:10.1016/j.molliq.2015.08.059

[28] I. A. W. Tan, B. H. Hameed, A. L. Ahmad, Equilibrium and kinetic studies on basic dye adsorption by oil palm fibre activated carbon, Chem. Eng. J., 127 (**2007**) 1, 111–119, doi:10.1016/j.cej.2006.09.010

[29] A. Khasri, O. S. Bello, M. A. Ahmad, Mesoporous activated carbon from Pentace species sawdust via microwave-induced KOH activation: optimization and methylene blue adsorption, Res. Chem. Intermed., (**2018**), 1–21, doi:10.1007/s11164-018-3452-7

[30] M. Baysal, K. Bilge, B. Yilmaz, M. Papila, Y. Yürüm, Preparation of high surface area activated carbon from waste-biomass of sunflower piths: Kinetics and equilibrium studies on the dye removal, J. Environ. Chem. Eng., (**2018**), 1702–1713, doi:10.1016/j.jece.2018.02.020

[31] Y. Wang, J. Pan, Y. Li, P. Zhang, M. Li, H. Zheng, X. Zhang, H. Li, Q. Du, Methylene blue adsorption by activated carbon, nickel alginate/activated carbon aerogel, and nickel alginate/graphene oxide aerogel: a comparison study, J. Mater. Res. Technol., 9 (**2020**) 6, 12443–12460, doi:10.1016/j.jmrt.2020.08.084